1   <u>**Revision 1**</u>

2   **Microprobe analysis and dating of monazite from the Potsdam**

3   **Formation, NY: A progressive record of chemical reaction and**

4   **fluid interaction**

5

6   Julien **Allaz**[1,2,*], Bruce **Selleck**[3], Michael L. **Williams**[1], Michael J. **Jercinovic**[1]

7

8   [1] Dept. of Geosciences, University of Massachusetts, Amherst, 611 North Pleasant Street, 233

9   Morrill Science Center, Amherst, MA 01003

10   * Corresponding author: julien.allaz@colorado.edu

11   [2] Present address: Geological Sciences, University of Colorado Boulder, UCB 399, 2200

12   Colorado Ave., Boulder, CO 80309

13   [3] Department of Geology, Colgate University, 13 Oak Drive, Hamilton, NY 13346

14

15

16   **Abstract**

17

18   It has been recognized for several decades that REE-phosphates (monazite and xenotime) can

19   grow during diagenesis and low-grade metamorphism. Growth of REE-bearing accessory

20   phases at low-grade conditions commonly involves pervasive fluid-rock interaction,

21   dissolution of detrital grains, transportation, and precipitation of REEs, typically facilitated

22   by an increase in temperature. The occurrence of low-grade REE-phosphate offers a rare

23   opportunity to date a crystallization/mineralization and possibly fluid percolation.

24   We report here the results of in situ dating by electron microprobe of Paleozoic

25   authigenic and low-grade monazite and xenotime overgrowths on detrital monazite and

26   zircon, respectively. Samples are from the Potsdam Formation, a basal sandstone deposited

27   uncomfortably on Proterozoic basement of the Adirondack Mountains of New York State.

28   This study also focuses on the textural and chemical relationships of these REE-bearing

29   accessory phases. Textures include rounded and fractured detrital monazite and zircon, which

30   contrast with new sub-euhedral REE-phosphate overgrowths. Monazite overgrowths are

31   enriched in LREE and depleted in HREE compared to detrital cores. The U and Th

32   concentrations are low, typical of low-grade metamorphic conditions.

33   Monazite core ages yield Proterozoic ages between 1.17 and 0.90 Ga (Shawinigan and

34   Ottawan orogeny). Monazite overgrowth and xenotime ages indicate four to five major

35   overgrowth events between ca. 500 Ma (shortly after the time of deposition) and ca. 200 Ma.

36   As these ages are relatively young and the actinide content is low ($\Sigma < 2$ wt.%), the

37   radiogenic Pb content of monazite overgrowths and xenotime is low (< 400 ppm). Therefore,

38   EPMA dates have relatively large uncertainties. Nevertheless, the ages determined broadly

39   correlate with major Paleozoic orogenic events recorded in the Appalachian Orogen to the

40   East (Taconic, Salinic, Acadian, Neo-Acadian and Alleghanian). Fluid percolation, driven by

41   orogenic loading, may induce dissolution of detrital monazite and zircon. Subsequent

42   precipitation of new monazite and xenotime probably results from changes in fluids or

43   metamorphic conditions. This study demonstrates the power of the EMPA technique to

44   resolve the fluid-related growth history of REE-phosphates in low-grade metasediments.

45

46

47   **Introduction**

48

49   Fluids play an important role in the evolution of sedimentary rocks from early diagenesis and

50   lithification to alteration, low-grade metasomatism, and even ore mineralization (e.g. Putnis

51   and Austrheim 2010). Fluids may be derived locally, during compaction and dewatering, or

52   they may be derived from underlying rocks or from deeper parts of the sedimentary basin

53   during burial or tectonic loading. Fluid-rock interaction can fundamentally modify the

54   original mineral assemblage(s), bulk composition, and mechanical properties, thus obscuring

55   the record of depositional environments and sedimentary provenance. However, fluid-rock

56   interaction can also leave an interpretable record of stages in the evolution of a sedimentary

57   basin and of depositional and tectonic events in other parts of the basin. It is important to

58   identify and characterize the spatial, temporal, and compositional nature of fluid-rock

59   interaction events, but this has proven to be challenging because of the relatively low

60   metamorphic grades and the heterogeneity of fluid pathways through many sedimentary

61   rocks.

62   Analysis and dating Rare Earth Element (REE) phosphate, i.e. monazite and

63   xenotime, is a promising approach for characterizing past fluid interaction events in

64   sedimentary rocks. Monazite (LREE-phosphate) and xenotime (HREE-phosphate) are

65   common detrital minerals in a variety of sedimentary rocks (Overstreet 1967). Further, they

66   are susceptible to dissolution and precipitation, and it has been recognized for several decades

67   that authigenic monazite can overgrow detrital monazite during diagenesis (Burnotte et al.

68   1989; Evans and Zalasiewicz 1996; Evans et al. 2002; Tomkins and Ross 2005), and also

69   during low-grade metamorphism (Cabella et al. 2001; Rasmussen et al. 2001; Rasmussen and

70   Muhling 2007; Wan et al. 2007; Wilby et al. 2007). The broad compositional range of

71   monazite and xenotime, including an array of trace elements and REE, make them very

72   suitable geochemical monitors. Further, both monazite and xenotime can incorporate

73   significant amounts of Th and U, with little common Pb, which makes them datable by

74   isotopic or elemental chemical analysis. Therefore, they provide an opportunity to monitor

75   the geochemical evolution through time of sedimentary basins (e.g. Burnotte et al. 1989;

76   Evans et al. 2002; Wilby et al. 2007; Mahan et al. 2010).

77   This paper presents results of an investigation of the evolution of REE-phosphates in

78   the Upper Cambrian Potsdam Formation (NY, USA). Several generations of monazite and

79   xenotime overgrowths are associated with detrital monazite and zircon, respectively. The

80   presence of these overgrowths provides an opportunity to date and characterize the diagenesis

81   and low-grade burial metamorphism in the Potsdam Formation. Here, we use the electron

82   microprobe to reveal variation of composition and U-Th-Pb age in situ, that is, on mineral

83   grains and overgrowths exposed in thin sections of the sedimentary rocks. Results indicate

84   that several distinct events, possibly linked to Appalachian orogenic pulses, have triggered

85   the dissolution and precipitation of REE-minerals.

86

87

88   Geological setting and sample description

89

90   The Potsdam Formation was deposited during Middle to Upper Cambrian (510-490 Ma;

91   Fisher 1977; Landing et al. 2009). It ranges from feldspar-rich arkose (basal Aussable

92   Member) to nearly pure quartzite (Keeseville Member). Sedimentary facies analysis indicates

93   a progressive change from terrestrial to shallow marine deposition (Fisher 1968). The

94   Potsdam Formation was unconformably deposited on Grenvillian metamorphic rocks of the

95   Adirondack massif (NY, USA; Ontario and Québec, Canada).

96   Samples were collected from six localities near the margins of the Adirondack massif

97   in New York State (Fig. 1). The sandstones consist of quartz and K-feldspar, with a matrix of

98   Fe-rich chlorite, quartz, illite, minor kaolinite and local carbonate (Selleck 2008). Heavy

99 minerals, including monazite, xenotime and zircon, are commonly concentrated along thin

100 placer laminae in coarse pebbly sandstone. Aside from late fracturing, no obvious

101 deformation features are visible in these samples.

102   Authigenic REE-minerals (monazite, xenotime), sulfides (pyrite, galena, sphalerite),

103 fluorite and barite suggest that hydrothermal fluids circulated through permeable basal sands

104 in the Potsdam Formation, causing alteration of susceptible minerals such as biotite,

105 hornblende, garnet, ilmenite, and plagioclase. Fluid inclusion data (homogenization and

106 melting temperatures) from Collins-Waite (1987) on vein quartz and carbonate suggest that

107 metamorphic temperatures were in excess of 200°C with high salinity, near halite saturation.

108

Methodology

110

111 Nine samples were selected for petrographic examination and microprobe analysis. Textural

112 and compositional relationships between detrital and authigenic minerals were examined.

113 Identification of zircon, monazite, and xenotime was performed by acquiring full-thin-section

114 Wavelength Dispersive Spectroscopy (WDS) maps of Zr Lα, Ce Lα and Y Lα on a

115 CAMECA SX-50 microprobe at the University of Massachusetts, following the method of

116 Williams and Jercinovic (2006). Then, high-resolution WDS maps of Th Mα, U Mβ, Y Lα,

117 Ca Kα and one REE (Nd Lα, Pr Lα or Sm Lα) were acquired from numerous monazite

118 grains in each polished section. For xenotime, Y Lα, Th Mα, U Mβ, Dy Lα and Gd Lα x-ray

119 maps were generated; Zr Lα was occasionally used to highlight the zircon on which xenotime

120 grew.

121   Quantitative analyses were acquired on the CAMECA SX-100 "Ultrachron"

122 microprobe at the University of Massachusetts, following methods described in Williams et

123 al. (2006) and Jercinovic et al. (2008) for monazite, and in Hetherington et al. (2008) for

124   xenotime. In addition to the interference corrections described in these papers, a correction

125   for the interference of Pr L$\beta_{2,15}$ on Eu Lα was included. Acquisition time for U (600 s), Th

126   (500 s) and Pb (700 s, integrating counts from two spectrometers equipped with VLPET

127   crystals) were optimized to improve precision and accuracy, while minimizing diffusion

128   effects. Background intensities for U, Th, and Pb were regressed from high-resolution WDS

129   scans (see Williams and Jercinovic 2006).

130   Standardization and age calculations were checked before and after each analysis

131   session using the following consistency standards: (a) Moacyr monazite (TIMS ^{207}Pb/^{235}U

132   506.7 ± 1.4 Ma and ^{208}Pb/^{232}U 506.4 ± 1.8 Ma; B. Davis, pers. comm. 2005) and (b) GSC-

133   6413 xenotime (TIMS ^{207}Pb/^{206}Pb 996.7 ± 0.8 Ma and ^{206}Pb/^{238}U 993.8 ± 0.7 Ma; Stern and

134   Rayner 2003). In addition to U, Th and Pb, monazite and xenotime analyses include Si, P, S,

135   Ca, As, Y and REE (La to Nd and Sm to Yb). Results are presented in Table 1, and the

136   complete set of analysis is available in Table DR1 in the Data Repository. U-Th-Pb dates

137   were calculated based on the age equation from Montel et al. (1996) and decay constants

138   from Steiger and Jäger (1977). We distinguish an analysis (single point measurement) from a

139   date, obtained by averaging 3 to 12 single point analyses in a homogeneous compositional

140   domain. Errors associated with dates are given at the 2σ level and include counting statistics

141   and a 10% relative error on the background regression.

142   The CAMECA SX-100 "Ultrachron" is optimized for U, Pb and Th acquisition.

143   However, the low actinide content and the Paleozoic age of these grains result in low total Pb,

144   typically between 22 and 392 ppm. This is close to the detection limit of the electron

145   microprobe at the optimum analytical conditions used here; the detection limit for Pb is ca. 10

146   ppm on a 5-point average. Longer counting time or higher current would improve this, but

147   the risk of inaccuracy due to beam damage would become unacceptable (see Jercinovic et al.

148   2012). Therefore, dating results show large variability even within single homogeneous

149   domains, and errors are typically larger than ±25 Ma (2σ). When Th and Pb concentration are

150   greater than 1.2 wt% and 250 ppm respectively, errors are less than ±20 Ma (ca. 5% relative).

151   There is no correlation between the calculated dates and Pb- or Th-content (Fig. 2a), but a

152   correlation exists between the relative error and the Pb- or Th-content (Fig. 2b).

153

154

155   **Results**

156

157   *Detrital monazite*

158

159   Monazite grains exposed in thin section are typically greater than 50 µm in size, and are

160   commonly concentrated on bedding planes with other heavy minerals (e.g. oxides, zircon).

161   On backscattered electron (BSE) images, most monazite grains have distinct bright cores and

162   darker rims. The cores are typically rounded and fractured. They commonly have patchy

163   zoning (Fig. 3f-l, n-q), but are typically rich in Th (3.5 to 22.0 wt-% ThO_2) and Y (0.1 to 4.2

164   wt-% Y_2O_3; Table DR1). Most cores have a significant component of cheralite (Chr;

165    $CaTh(PO_4)_2$) and thorite/huttonite (Thr; $(Th,U)SiO_4$), with up to 30-40% Thr+Chr in grain

166   m1 of sample EC-3, and 10-15% in all other samples (Fig. 4a). REE spectra vary from

167   sample to sample and within a single sample (Fig. 5b; Fig. DR1). Dates fall into a number of

168   sub-populations but are constrained between 1005 and 1162 Ma with errors between 5 and 13

169   Ma (2σ; Tables 1, DR1; Fig. 6).

170

171   *Monazite overgrowths*

172

173   Monazite overgrowths commonly surround detrital monazite cores. The overgrowths are

174   typically 50-100 μm in apparent thickness, resulting in very large (for accessory minerals)

175   composite grains, up to 200-300 μm. Smaller overgrowths of 5-50 μm are also observed.

176   When present, the overgrowths represent 30 to 70% of the total grain area. They are typically

177   in optical continuity with the detrital cores (Fig. 3d). The overgrowths are texturally distinct

178   from the rounded and locally fractured cores. They typically have subeuhedral crystal shapes,

179   but they can also fill cracks and grain interfaces. Apatite, $ThSiO_4$, and/or xenotime commonly

180   occur along the core-rim interface or along fractures in cores.

181   Some overgrowths are incomplete or asymmetric in their distribution around detrital

182   cores. Many are preferentially developed towards pore space, or susceptible minerals such as

183   plagioclase or K-feldspar. Textural analysis further suggests a preferential replacement of K-

184   feldspar by monazite relative to other matrix phases, as shown in Figure 7a,b; the overgrowth

185   contains inclusions of K-feldspar, whereas the overgrowth is much thinner or absent when

186   adjacent to quartz or other less soluble minerals.

187   Overgrowths typically display multiple concentric layers, each with a distinct

188   composition (e.g. Fig. 3). Successive rim analyses are identified with by number; "rim1"

189   being the innermost, nearest to the core (Table DR1). WDS compositional mapping of Nd Lα

190   notably reveals distinctive compositional textures. The innermost overgrowth typically has a

191   fibrous or floweret texture, with fibers radiating from the core-overgrowth interface (e.g. Fig.

192   3a,e). Monazite "fibers" are also rarely found as overgrowths on zircon (Fig. 7c). The next

193   successive overgrowth generation typically fills the spaces between the rim1 fibers (Fig. 3a-

194   c). Subsequent generations occur in concentric layers. Up to 4 layers have been distinguished

195   in a single grain (e.g. LM-11 m1 in Fig. 3a-c). Up to 5 compositionally distinct layers have

196   been identified among several grains in a single sample.

197   REE spectra from monazite overgrowths are distinctly different from those of the

198 cores (Fig. 5). Although absolute values differ from grain to grain, all rims are depleted in Th,

199 U, Y, Ca, Si and HREE compared to cores, and slightly enriched in light REE (LREE; La to

200 Eu; Table DR1; Figs 3,4b). A positive correlation between Nd, Pr, Sm, Gd, Eu and Tm is

201 observed, while La and Ce are anti-correlated with these elements. These observations are

202 independent of sample locality, with the exception of the PC samples, which tend to yield the

203 highest La-contents and also higher La/Nd ratios relative to other samples. Whereas all

204 detrital monazite cores show a negative Eu-anomaly, most overgrowths do not (Fig. 5). U

205 concentrations are typically below detection limit (< 50-60 ppm), while Th and Y are low

206 (0.22 to 1.73 wt-% Th; 0.08 to 0.51 wt-% Y). Samples WNR-1 and WNR-3 contain sulfates

207 (barite, anhydrite/gypsum), and a significant amount of sulfur is detected in monazite,

208 especially in rims (cores: 0.18-0.43; rims: 0.22-0.70 wt-% SO_2).

209   Dating results are represented graphically using a single Gaussian probability curve

210 for each homogeneous compositional domain, identified from high-resolution WDS maps (as

211 per Williams et al., 2006). Results for monazite range from 550 Ma to 320 Ma, with a few

212 outliers as young as 221 Ma (sample WFR-14 only) and as old as 745 Ma (Table DR1). Four

213 major peaks are visible in the combined data set for all samples: 505, 460, 420 and 370 Ma

214 (Fig. 8a). Consistent with the concentric growth patterns, dates become progressively

215 younger from internal rims (500-400 Ma) to external rims (400-300 Ma). Figure 3a-d shows

216 an example with four compositional domains: (a) internal rim at 507±26 Ma, (b) two

217 intermediate domains at 418±20 Ma and 348±22 Ma, and (c) an external rim at 321±22 Ma.

218 Another spectacular overgrowth (m7 in sample PC-2A) has an internal rim at 528±26 Ma and

219 an external rim at 359±37 Ma (Table DR1). Some other rims only record one or two events

220 (e.g. PC-6 m3, one event: 436±30 and 402±61 Ma; Fig. 3e-g).

221   There is a noticeable difference in overgrowth geochronology between samples from

222   different geographic localities. Maxima for the northern (LM, EC; Fig. 1) and southern

223   (WNR; Fig. 1) samples occur at 420, 370 and 325 Ma, whereas maxima for eastern samples

224   (PC, WFR occur at 505, 460 and 420 Ma (Fig. 1). Further, even within a single sample,

225   contemporaneous (based on the age results) rims do not tend to have identical compositions,

226   although this could result from the large error on age, and the relatively small number of

227   grains analyzed. Several vague trends are apparent. With decreasing age:

228   • Y increases and Ce decreases (EC-3, LM-11, WFR-14 and WNR-3);

229   • Pr decreases (LM-12 and WFR-14);

230   • Eu and Gd slightly increase (LM-11, WFR-14 and WNR-3).

231   Interestingly, Th concentrations are highest in monazite with ages around 500-400 Ma for

232   several samples (Fig. 2a). The relatively high Th abundance also corresponds to relatively

233   high Ca, Sr and Y content (EC-3 and PC-2A).

234

235

236   *Xenotime*

237

238   Xenotime preferentially occurs as 10-30 µm-wide rims on detrital zircon grains. The

239   overgrowths are locally detached and separated from the zircon core, with the gaps primarily

240   filled with chlorite, illite and/or quartz (Fig. 9). Several minute grains up to 10 µm in

241   diameter also occur at the boundary between detrital monazite cores and overgrowths or

242   within fractures in monazite cores (Fig. 3c,e). 10-20 µm crystals occur more rarely in pore

243   spaces, between detrital quartz and feldspar. High-resolution WDS mapping and

244   compositional analysis reveals only subtle compositional zonation, particularly in Th, Y, Gd,

245   Dy, Er and Yb (e.g. Fig. 9 inset). Th-content is similar to monazite rims or slightly greater

246   (0.41 to 2.29 wt-% ThO_2), whereas U-content is significantly greater (0.12 and 0.30 wt-%

247   UO_2). Four age peaks are visible in the combined xenotime dataset: ca. 395, 370, 325, and

248   225 Ma (Fig. 8c). In contrast to monazite overgrowths, there are no xenotime dates in the

249   range of 505 and 460 Ma.

250

251

252   **Discussion**

253

254

255   ***Monazite cores***

256

257   Monazite cores are rounded, consistent with erosion and transport. REE patterns are strongly

258   variable from sample to sample and within a single sample (Fig. 5), reflecting their different

259   source regions or host rocks. Several monazite cores have patchy zoning indicative of fluid-

260   related alteration (e.g. Fig. 3f-l, n-q). Xenotime and $ThSiO_4$ (thorite or huttonite) are present

261   in cracks and on core to rim boundaries (Fig. 3g-h,o-p,s-t). Age results for some pristine cores

262   (Table DR1; Fig. 3a,r) demonstrate the usefulness of detrital monazite dating to illuminate the

263   origin of sediments (e.g. Hietpas et al. 2010). Most dates fall between 1.06 and 1.00 Ga,

264   characteristic of the Ottawan phase of the Grenville Orogeny (Wong et al. 2011). One core

265   yields 0.91±0.01 Ga (PC-6 m1, core 2; Fig. 6), and likely represents a later event following

266   the Ottawan Orogeny such as late granite intrusion, or retrograde metamorphism after the

267   Rigolet Orogeny (1005-980 Ma; McLelland et al. 2010). Two other cores yield 1.10 (LM-11

268   m1, core) and 1.16 Ga (PC-2A m2, core2; Fig. 6), which may be related to the Hawkeye

269   granite in LM samples (1100-1095 Ma) and to mangerite-charnockite intrusions in PC

270   samples (1160-1145 Ma; McLelland et al. 2010).

271

272

Monazite overgrowths

274

275   Monazite core-rim textures can be interpreted in terms of several different processes. They

276   might represent replacements (by metasomatism or alteration) of the outer parts of detrital

277   grains. Alternatively, they could result from precipitation of new monazite on precursor

278   grains. Both processes would indicate some degree of fluid-rock interaction, and both are

279   certainly enhanced at higher temperature. Several lines of evidence point to dissolution-

280   precipitation of new monazite overgrowths in our samples. First, a subeuhedral habit and

281   well-defined concentric zoning are visible on some compositional maps (e.g. Fig. 3i,r), This

282   texture, similar to magmatic monazite, is commonly observed in low-grade monazite

283   (Burnotte 1989; Shandl and Gorton 2004). Second, if monazite overgrowths were formed by

284   alteration/replacement (a pseudomorphic reconstruction mechanism), one would expect the

285   grain shape to preserve the original rounded and fractured shape of detrital grains and the

286   inner boundary to be more of an irregular reaction front (e.g. Petrík and Konecný 2009;

287   Hetherington et al. 2010), which is not the case. Third, monazite overgrowths are locally

288   developed on other detrital minerals, such as plagioclase and K-feldspar (e.g. Fig. 7a,b).

289   The presence of fluid circulation in the Potsdam Formation after deposition is

290   indicated by the presence of hydrous minerals (chlorite, clay) replacing feldspar and other

291   susceptible minerals. Fluid inclusion studies (Collins-Waite 1987; Lim et al. 2005), the

292   presence of chlorite and illite (Reynolds and Thomson 1993; Selleck 2008) and the conodont

293   alteration index of ca. 4 (Repetski et al. 2008) all document low-grade metamorphism and

294   metasomatism in the Potsdam Formation at ca. 250 °C. Further, zircon fission track dating

295   from the Potsdam and Galway Formations yield peaks at 540, 780 and 1200 Ma (Montario

296   and Garver 2009), i.e. older than the deposition time. This suggests that the sediments were

297   not heated above 200-300°C for extended periods. Peak pressures were on the order of 0.2

298   GPa, based on estimates of overlying sediment thickness (<7 km; Friedman 1987). At these

299   low-grade PT-conditions, volume diffusion is too sluggish to explain the observed

300   metamorphic reactions (e.g. chloritization of ferromagnesian silicate, sericitization of

301   feldspar). K-Ar modeling in K-feldspar suggests at least three thermal peaks at 470, 450 and

302   300 Ma (Heizler and Harrison, 1998). The low-grade reactions, and the growth of Paleozoic

303   REE-phosphate are thus interpreted to reflect fluid-rock interaction and dissolution-

304   precipitation (Putnis and Austrheim 2010). In addition, episodic fluid percolations are likely

305   to bring heat from deeper units, thereby increasing the reaction rate.

306   Monazite and xenotime results indicate a multiphase crystallization history. Based on

307   composition and U-Th-Pb dating, at least five discrete overgrowth generations were

308   identified, suggesting a minimum of five crystallization events. However, significant

309   questions include: the nature of the reactions involved in the formation of these REE-

310   phosphates, the possible source(s) for the REE, the origin and composition of the fluids

311   responsible for their growth, and finally, the possible causes of the fluid influx events. These

312   will be discussed in subsequent sections.

313

314

315   *Interpretation of Age Peaks*

316

317   Monazite and xenotime overgrowth ages are summarized in cumulative age probability

318   diagrams built from the summing of Gaussian probability curves for each set of analyses

319   (Fig. 8). The peaks for monazite (Fig. 8a,b) suggest five discrete pulses at 505, 460, 420, 370,

320   and 225 Ma. These pulses can be grouped in three main categories: (a) diagenetic (i.e. close

321   to the deposition time at 510-490 Ma), (b) older (470-420 Ma) and (c) younger ages (410-320

322   Ma). Only two samples yield even younger ages around 250-200 Ma (EC-3, WFR-14). The

323   results are consistent with results from Storm and Spear (2002), who report monazite rim

324   ages between 505 and 395 Ma, and allanite rim ages at 353 and 144 Ma in pelitic samples

325   from the southern Adirondack Mountains.

326   The peak distribution of monazite dates is different depending on the sample location

327   (Fig. 8b). The distribution of the older age group (470 to 420 Ma) is higher in the PC area (E-

328   side of the Adirondacks) than in the LM or EC areas (NE-side), while younger ages at 410

329   and 320 Ma are more common in the LM and EC areas. This suggests that crystallization of

330   REE-phosphate was more significant between 470 and 420 Ma in the E-flank of the

331   Adirondacks. Later generations, younger than 420 Ma, are more abundant in samples from

332   the northeastern flank of the Adirondacks.

333   Most xenotime dates correspond with the younger monazite groups, with two major

334   pulses around 350 and 225 Ma (Fig. 8c). Interestingly, xenotime overgrowths are detached

335   and separated from their original zircon substrate in some samples, and the space is filled

336   with metamorphic minerals (chlorite and illite; Fig. 9). The youngest xenotime with this

337   feature is 320±50 Ma (Fig. 8c). We conclude that low-grade metamorphic conditions

338   persisted or were reestablished periodically until 320 Ma. The late occurrence of xenotime

339   compared to monazite remains difficult to explain without precise fluid composition and

340   metamorphic conditions achieved during each event. We can only speculate that the level of

341   enrichment in HREE required for xenotime crystallization was higher during later events.

342   The problem of excess ^{230}Th (an intermediate decay product of ^{238}U; Schärer 1984;

343   Parrish 1990) cannot be addressed, because the isotope ratios are unknown in our data set.

344   Excess Th can be important in young monazite (< 500 Ma) with a high Th/U ratio. This will

345   induce an excess ^{206}Pb, which results in abnormally old microprobe dates. Although it is

346   impossible to estimate the magnitude of this effect, we suspect that it is within the large

347   analytical error for our samples.

348

349

350   *Orogenic loading and monazite crystallization*

351

352   REE-phosphates from the Potsdam Formation record four to five distinct crystallization

353   events (Fig. 8). Although some of the dissolution/precipitation events may have been

354   triggered by thermal pulses alone (with fluid derived from dehydration reactions), it seems

355   likely that crystallization was enhanced by the infiltration of external fluids (fluid pulses) that

356   would not only contribute heat, but also the necessary conditions for dissolution/precipitation

357   (pH, salinity…). The ages shown in Figure 8 broadly correlate with the age of diagenesis and

358   with the age of major orogenic events recorded in the Appalachian Belt to the east: diagenesis

359   (510-490 Ma; Fisher, 1977; Landing et al., 2009), Taconic (480-455 Ma), Salinic (445-420

360   Ma), Acadian (420-400 Ma), Neo-Acadian (380-350 Ma; van Staal et al. 2009), and

361   Alleghanian (310-250 Ma; Rast 1984; Wintsch et al. 2003; Walsh et al. 2007). We suggest

362   that each event recorded in monazite (after diagenesis) may be related to orogenic loading to

363   the east in the Appalachians Mountains, each of these loading events being accompanied by a

364   thermal pulse as suggested in Heizler and Harrison (1998), and a fluid pulse, also suggested

365   by fluid inclusion data (Table 2 and reference therein; see also discussion on dissolution-

366   reprecipitation). The youngest ages around 250-200 Ma from sample EC-3 and WFR-14 may

367   further reflect fluid flow and distal deformation associated with the breakup of Pangea.

368   Existing geochronologic constraints on orogenic loading in the Potsdam Formation

369   are rare. Beside data from Storm and Spear (2002), only illite K/Ar ages from the Potsdam

370   Formation around Alexandria Bay are available. Data from Reynolds and Thomson (1993)

371   yield 360 ± 9 Ma and 392 ± 9 Ma, and an unpublished K/Ar date by Selleck yields 355 ± 12

372   Ma. These also might suggest that low-grade metamorphism may be distally related to the

373   Neo-Acadian orogeny (395-350 Ma; van Staal et al. 2009). However, considering the range

374   of ages from monazite and xenotime preserved here, and the likelihood of several burial-

375   exhumation events between 500 Ma and 200 Ma around the Adirondack Mountains (e.g.

376   Heizler and Harrison 1998), another explanation may be the effect of mixed ages. The

377   occurrence of several illite generations or partial resetting of K-Ar is likely, and would result

378   in the observed distribution of K/Ar ages.

379   We also observe that older ages are more common in monazite from PC samples (Fig.

380   8b). These observations are consistent with studies on extensional structures in and around

381   the Taconic allochthon near Whitehall (Goldstein et al. 2005; Lim et al. 2005): Taconic veins

382   (480-455 Ma) are more common than Acadian or later ones (younger than 420 Ma), and most

383   Taconic faults were not reactivated during the Acadian orogeny. Moreover, homogenization

384   temperatures of fluid inclusion are lower in Acadian veins compared to Taconic veins. The

385   close proximity of PC samples to the Taconic frontal thrust may explain this difference. Other

386   samples, situated north and south of the Adirondack Mountains, are further from the Taconic

387   frontal thrust. Although there are no detailed studies of fault distribution and timing in the

388   northern area near the LM and EC samples, several large scale faults are known to have been

389   reactivated during the Acadian orogeny (Jacobi 2002), and could have induced fluid flow in

390   sediments lying on the NE-side of the Adirondacks, thus promoting the growth of younger

391   monazite.

392
393

394   ***Source of REE***

395

396   All monazite overgrowths in the Potsdam samples studied here are characterized by

397   enrichment in LREE, depletion of HREE, Y, and actinides, and also have a higher Eu

398   concentration compared to the detrital cores (Table DR1; Fig. 4). Studies on authigenic and

399   low-grade monazite have suggested several possible sources of REE: (a) REE adsorbed on

400   clay minerals (Burnotte et al. 1989; Milodowski and Zalasiewicz 1991), (b) liberation of REE

401   during the reduction of Fe-oxides and hydroxide (Milodowski and Zalasiewicz 1991; Lev et

402   al. 1998), (c) degradation of organic matter (Evans and Zalasiewicz 1996; Lev et al. 1998),

403   and (d) dissolution of existing REE-rich minerals such as allanite, monazite, or xenotime

404   (Janots et al. 2008; Rasmussen and Muhling 2009). Cases (a) and (b) are likely to occur

405   during the early growth of REE-phosphate, i.e. during burial and diagenesis. However, case

406   (b) remains uncertain because the observed mineralogy suggests a slightly oxic environment;

407   Fe- and Ti- (hydr-) oxides are present together with sulfate, whereas sulfides are only present

408   in the basal layers of the Potsdam Formation. Case (c) seems unlikely due to the absence of

409   significant organic matter in the Potsdam samples. Textures in the Potsdam samples suggest

410   that the most plausible explanation is that detrital monazite is the major source of REE during

411   low-grade metamorphism (case d). Therefore, we suggest that growth of Paleozoic monazite

412   in the Potsdam Formation involves mainly the dissolution of detrital monazite, followed by

413   transportation, and later precipitation. The following non-stoichiometric reaction is

414   suggested:

415

416    $\text{Mnz}_1 + \text{Fsp} \pm \text{Ap} \pm \text{Grt} \pm \text{Zrn} + \text{Fluid}_1 \Leftrightarrow \text{Mnz}_2 + \text{Xnt} + \text{Thr} \pm \text{Ap} \pm \text{Chl} \pm \text{clay} + \text{Fluid}_2$ (1)

417

418   This reaction involves the dissolution of detrital monazite (Mnz_1) and feldspar (Fsp), which

419   releases P and LREE into the solution. The general increase of Eu anomaly (Eu/Eu*)[1]

420   between detrital and overgrowth monazite is attributed essentially to feldspar breakdown,

421   especially plagioclase. Eu/Eu* values increase dramatically between detrital monazite (ca.

422   0.1-0.2) and monazite overgrowths (0.55-1.45 Eu/Eu*; Table DR1). Eu/Eu* is higher for LM

423   samples and for some WNR monazite, which is consistent with the presence of strongly

424   sericitized plagioclase, particularly in LM samples, that may have released Eu into the fluid.

425   Garnet (Grt), zircon (Zrn) and other susceptible minerals potentially provide additional

426   HREE in the fluid.

427   Once saturated in REE or upon a change in fluid conditions, new monazite enriched

428   in LREE (Mnz_2) is precipitated. Detrital apatite (Ap) could provide an additional source of P,

429   and could also re-precipitate later when the solution becomes undersaturated in REE. The

430   REE budget is balanced by the growth of xenotime taking most of the Y+HREE (Fig. 3h,p.t),

431   and also $ThSiO_4$ for the actinides ($\pm$Y; Fig. 3g,o,s), both minerals crystallizing mainly around

432   and in fractures of detrital cores. Although no well-constrained analyses were obtained from

433    $ThSiO_4$, due to the fine grain size (typically a few micron or less), analysis of grains in PC-6

434   reveals a maximum of 1-2 wt% U. Because new monazite and xenotime are poor in actinides,

435    $ThSiO_4$ is the main secondary phase that contains most of the actinides released by the

436   dissolution of detrital monazite. However, the Th/U ratio in $ThSiO_4$ is higher than that of

437   several monazite cores, suggesting that some U remains in solution (see concluding remarks).

438   The breakdown of feldspar and other silicates is balanced by the growth of chlorite

439   (Chl) and clay minerals (illite or illite/smectite). Other silicates might also be involved in this

440   reaction (e.g. amphibole, mica, oxide, hydroxide). The difficulty of accurately determining

---

[1] Eu/Eu* = $Eu_{CI}/(Sm_{CI} * Gd_{CI})^{0.5}$; CI = normalization to carbonaceous chondrite from McDonough and Sun 1995).

441   the modal abundance of accessory phases prevents an accurate mass balance calculation.

442   Moreover, the relative transport distance of the REE-enriched fluid remains unknown, and

443   the system is likely to have been open.

444   Fluid-mediated reactions seem most likely (e.g. Putnis and Austrheim 2010), because

445   the metamorphic conditions never exceed lower greenschist facies, and diffusion rates are

446   expected to have been low. This is also supported by the presence of hydrous phases

447   replacing plagioclase and K-feldspar (e.g. chlorite, illite), and more indirectly by the

448   occurrence of hydrothermal veins interpreted to be related to Paleozoic orogenies (e.g.

449   Collins-Waite 1987; Goldstein et al. 2005; Lim et al. 2005). The precise conditions of

450   dissolution-transport-precipitation are difficult to assess, but REE-phosphate chemistry, fluid

451   inclusion studies, and studies on REE speciation in low-grade fluids are helpful. In the

452   following section, we speculate on the possible fluid composition ($Fluid_1$) associated with

453   each growth phase.

454   The composition of monazite overgrowth generations varies slightly from sample to

455   sample. Further, correlations between LREE (Ce, La, Nd) and MREE (Pr, Sm, Gd) may

456   reflect a change in pressure, temperature, or fluid conditions (composition, pH, eH).

457   Composition of co-genetic monazite (based on age data) even in a single sample is variable

458   from grain to grain (Table DR1). If the composition of an infiltrating fluid was the dominant

459   control on the composition of new monazite, one would expect it to be homogeneous

460   throughout a specific sample. Instead, the variation seems to suggest local derivation of REE

461   from detrital monazite, which in turn, influences the fluid composition. A strong effect of

462   local rock composition, and thus, partial disequilibrium and lack of homogenization at the

463   thin section scale, is indeed expected for low-grade metamorphism, especially for REE (e.g.

464   Carlson 2002; Vidal et al. 2006).

465

466

467 *Dissolution-precipitation of REE-phosphates*

468

469 The oldest monazite overgrowths in the Potsdam Formation yield ages close to the time of

470 deposition (ca. 510-490 Ma; Fisher 1977; Landing et al. 2009). These overgrowths are

471 usually thinner compared to younger ones. In a few grains, such as m1 in LM-11 (rim1:

472 507±26 Ma), finger-like or floweret structures are visible in Nd and Sm maps (Fig. 3a,e). A

473 similar fibrous texture is also observed in a monazite overgrowth on zircon (e.g. Fig. 7c).

474 This habit suggests that the precursor of monazite may have been rhabdophane

475 (hydrophosphate), a diagenetic mineral that commonly occurs in fibrous aggregates (e.g.

476 Milodowski and Zalasiewicz 1991; Lev et al. 1998; Čopjaková et al. 2011). However, Akers

477 et al. (1993) suggested that rhabdophane is unlikely to be the precursor of monazite.

478 Schatzmann et al. (2009) observed floweret crystals of $LaPO_4$ precipitating from

479 $La(NO_3).6H_2O$ and phosphoric acid reaction at low temperature, so this texture may be

480 common to early monazite growth during low-temperature diagenesis.

481 Early burial could also have caused an increase in temperature during diagenesis, but

482 in the absence of constraints on the early burial history of the Potsdam Formation in the area

483 studied, this hypothesis remains to be tested. Fluids may have played a more important role in

484 the early precipitation of monazite; studies on low-grade "authigenic" monazite have

485 suggested that the release of pore water, the dehydration of clay minerals, and/or the

486 infiltration of meteoric water could have induced the initial precipitation of monazite at ca.

487 510-490 Ma (e.g. Milodowski and Zalasiewicz 1991; Evans and Zalasiewicz 1996;

488 Rasmussen et al. 2001; Čopjaková et al. 2011). In contrast to black shale and mud rock (e.g.

489 Evans et al. 2002; Wilby et al. 2007), the Potsdam Formation has very little organic matter,

490 and the presence of hydrocarbon is unlikely at this stage in the burial history. No xenotime of

491   this age has been identified. This suggests that (a) xenotime was unstable during early burial,

492   (b) the fluid was mostly saturated in LREE, or (c) the amount of xenotime produced was too

493   small to be identified and/or that it was dissolved during a later event.

494   The presence of hydrous minerals (chlorite, illite), together with calcite, sulfate and

495   other diagenetic minerals in the Potsdam Formation suggests low-grade metamorphism

496   reaching a maximum of 250°C. Fluid-inclusion studies, summarized in Table 2, provide some

497   constraints on the possible fluid composition and temperature (Collins-Waite 1987; Elliott

498   and Aronson 1987; Whitney and Davin 1987; O'Reilly and Parnell 1999; Goldstein et al.

499   2005; Lim et al. 2005). Fluids associated with thrusting during the Taconic orogeny yield low

500   salinity and variable homogenization temperatures pointing to maximum temperature

501   between 170 and 280°C (Lim et al. 2005; Goldstein et al. 2005). These fluids are likely to

502   have originated from the dehydration of clay minerals (e.g. Milodowski and Zalasiewicz

503   1991; Lev et al. 1998; Goldstein et al. 2005). Variable salinity in the range 5-12% NaCl

504   equivalent is observed in samples close to the carbonate platform due to the mixture of water-

505   rich fluid with saline fluid from the carbonate platform (Lim et al. 2005). During the Acadian

506   and Neo-Acadian orogenies (420-350 Ma), fluid temperature decreased to 145-225°C and

507   salinity increased up to 21% equivalent NaCl due to the possible reflux of Silurian evaporite

508   brines (Collins-Waite 1987). Finally, during the Alleghanian orogeny (310-250 Ma), highly

509   saline and medium-warm (70-130°C) fluids induced further clay transformation in the

510   southern Appalachians (illitization; Elliott and Aronson 1987). This is possibly accompanied

511   by hydrocarbon enrichment (O'Reilly and Parnell 1999).

512

513

514   *REE speciation*

515

516   Several studies have investigated the speciation of REE in sediments at variable temperature,

517   pH, eH, and fluid composition (McLennan 1989; Haas et al. 1995; Lewis et al. 1997; Lev et

518   al. 1998, 1999; Gimeno Serrano 2000; Smith et al. 2000). Fluoride, chloride and hydroxide

519   create REE complexes at low, neutral and high pH, respectively (Haas et al. 1995). There is

520   no evidence in the literature for F-rich fluid percolating in the Potsdam Formation and other

521   Paleozoic units, and therefore it is likely that Cl-content in fluid and pH play a major role in

522   REE speciation. From the fluid-inclusion data presented above, an increase in fluid salinity

523   was observed between Taconic and Neo-Acadian orogenies (i.e. from 510 to 350 Ma; Table

524   2). In addition, fluids were significantly hotter around PC and WFR samples, up to 280°C

525   (Collins-Waite 1987; Lim et al., 2005); these warmer and more saline fluids would have

526   enhanced REE-dissolution, which is consistent with the prominence of Taconic ages in

527   monazite overgrowths from PC and WFR samples (warmer fluid) and of Acadian or Neo-

528   Acadian ages in those from EC and LM samples (higher fluid salinity; Fig. 8b). The

529   formation of carbonate complexes may further enhance the dissolution of REE in the form of

530   bicarbonate (REE-HCO$_3^{2+}$) or carbon trioxide (REE-CO$_3^+$) depending on pH (Haas et al.

531   1995). A slightly higher La/Nd ratio in monazite overgrowths from PC and WFR samples

532   further suggests interaction with carbonate-bearing fluid (e.g. Smith et al. 2000).

533   The larger volume of monazite overgrowths compared to xenotime, and the depletion

534   of HREE in monazite overgrowths compared to cores can be further explained by the

535   presence of Cl, which preferentially creates complexes with LREE (Haas et al. 1995). This

536   may also explain the scarcity of xenotime compared to monazite. REE can also be dissolved

537   through interaction with sulfate complexes (Lewis et al. 1997; Gimeno Serrano 2000). This is

538   likely the case for WNR samples, where sulfates are present, and monazite shows a

539   significant amount of S (Table DR1). Finally, hydrocarbon-rich fluids are likely to release

540   additional REE into fluids (e.g. Lev et al. 1998), and to further induce new monazite

541   crystallization during the Alleghanian orogeny (310-250 Ma) where hydrocarbon-rich fluids

542   have been documented (O'Reilly and Parnell 1999). More details on fluid REE-enrichment

543   and precipitation necessitate more accurate fluid composition data. Another unknown is the

544   exact pH of these fluids; a lower pH might have enhanced the dissolution of REE-minerals

545   (Lewis et al., 1997), but in the absence of specific fluid composition data this remains

546   elusive. Despite the limited knowledge of fluid composition, we conclude that the solubility

547   of REE in the Potsdam Formation is essentially triggered by an increase in temperature and

548   fluid salinity, whereas a decrease of temperature during (partial) exhumation would induce

549   precipitation. Locally, sulfur-, carbonate- or hydrocarbon-rich fluids are potential candidates

550   for enhancing dissolution of detrital monazite.

551

552

553   *The role of feldspar*

554

555   Finally, some monazite rims appear to grow into K-feldspar (thickest rim adjacent to K-

556   feldspar; Fig. 7a,b). This disequilibrium texture further implies a strong interaction with a

557   fluid that promotes metasomatism and dissolution-precipitation as described in Putnis and

558   Austrheim (2010). Plagioclase is also altered, and participates in the monazite forming

559   reactions through the release of Eu in fluid and the enrichment in Eu in monazite overgrowths

560   compared to cores (Fig. 5). These features suggest that (a) monazite rims preferentially grow

561   toward susceptible minerals, and (b) the dissolution of alkali in fluids could enhance the

562   process of monazite dissolution and precipitation. The latter has been demonstrated

563   experimentally at both low and high PT-conditions (Chisca et al. 2009; Harlov et al. 2011).

564   The dissolution of K-feldspar or plagioclase is expected to increase the alkali-content

565   in solution, inducing a local increase of pH. Experiments on REE-speciation at different pH

566   demonstrate a strong diminution of REE-solubility at near-neutral conditions (e.g. Lewis et

567   al. 1997; Oelkers and Poitrasson 2002; Poitrasson et al. 2004). A sudden neutralization of

568   fluid acidity through K-feldspar dissolution could induce the precipitation of REE-minerals.

569   However, clays (e.g. illite) also locally replace the feldspar, and this reaction would tend to

570   buffer the pH and the fluid alkalinity. Dissolution and precipitation may reflect the local

571   balance of conflicting influences on fluid pH and fluid composition.

572

573

574   **Concluding remarks**

575

576   The study of accessory phases, notably REE-phosphate, in low-grade sediments has a great

577   potential not only to date but also to provide a qualitative and quantitative characterization of

578   fluid infiltration in sedimentary units. Obviously, more work is required on this subject and is

579   beyond the scope of this paper. The electron microprobe offers high-spatial resolution in situ

580   dating of these micrometer-sized overgrowths. However, the technique has its limitations,

581   notably in terms of precision and accuracy, dictated by the detection limits of U, Th, and Pb

582   measurements, and by the potential for excess ^{230}Th (Schärer 1984; Parrish 1990) particularly

583   in younger monazite. Laser ablation or isotope dilution techniques could potentially

584   overcome this issue, but these techniques will likely yield mixed ages, because most of the

585   monazite grains have multiple narrow (5-10 μm) overgrowth domains with relatively

586   complex geometry.

587   The process of dissolution-precipitation of REE-phases is still subject to several

588   unknowns. It is crucial to have a better knowledge of fluid conditions (temperature, pH, eH,

589   composition) associated with the process of dissolution-precipitation, and in this sense, fluid

590   inclusion data could be extremely useful (e.g. Smith et al. 2000). Although no fluid inclusion

591   data have been collected for our samples, the composition of REE-phases can be used as a

592   qualitative indicator of fluid conditions. The REE-pattern of monazite indicates Y, HREE, Th,

593   and U depletion, compensated by LREE enrichment. Xenotime is also typically poor in

594   actinides, although slightly richer in Th and U compared to monazite in these samples; the

595   REE-budget is dominated by HREE. These results imply that the REE-pattern of a

596   sedimentary rock can be strongly affected by fluid percolation, which calls into question the

597   use of REE-patterns as indicators of sediment provenance (McLennan 1989). To assess the

598   precise conditions of leaching in sedimentary environments, further investigations combining

599   bulk-rock geochemistry, fluid inclusion data, and modeling of REE-speciation under variable

600   fluid conditions is required.

601   Finally, the results of the study have implications for the use of phosphates in nuclear

602   waste storage. REE-phosphates are thought to be candidates for nuclear waste storage (e.g.

603   Ewing and Wang 2002; Oelkers and Montel 2008; Chisca et al. 2009), as they can contain

604   significant amounts of actinides, are resistant to metamictization, and have a fast recovery

605   from damage induced by alpha particles. However, several studies at lower PT-conditions

606   have demonstrated that alkali-rich fluid, notably KOH fluids, can potentially alter monazite to

607   an amorphous phase, as can HCl and humic acid commonly found in soil (e.g. Chisca et al.

608   2009; Polyakov et al. 2010). Our study and other field studies have highlighted the potential

609   for hydrothermal alteration or dissolution-reprecipitation of REE-phosphates under

610   geological conditions that would approach those of long-term storage for nuclear waste (e.g.

611   Poitrasson et al. 1996, 2000; Read et al. 2002). Although the exact timing for such reactions

612   remains largely unknown, the rapid rate of experimental reactions showing dissolution-

613   reprecipitation of monazite at 300-500 °C (e.g. Harlov et al. 2007; Williams et al. 2011)

614   suggests that reaction progress under natural conditions could be very rapid. An important

615   point is that newly formed monazite in the fluid rich diagenetic environment is poor in

616   actinides relative to associated and partially dissolved detrital monazite. Whereas most of the

617   Th from detrital monazite appears to reprecipitate as $ThSiO_4$, the fate of U remains less

618   certain. Both $ThSiO_4$ (Th/U = 20-718) and monazite overgrowths (Th/U = 34-620) in sample

619   PC-6 yield higher Th/U ratios compared to monazite cores (Th/U = 5.5-90), which would

620   suggest that U partly remains in solution. This observation is further supported by

621   experiments at high pH, which progress eventually to the reprecipitation of Th minerals, and

622   U enrichment of the fluid (Clavier and Dacheux 2006). Monazite is certainly better than a

623   glass matrix for actinide storage (Oelkers and Montel 2008), but further research regarding

624   the short-term (laboratory time scale) and long-term (natural field time scale) behavior of

625   monazite under hydrogeological conditions is clearly warranted.

626

627

Acknowledgments

629

635

636

References

638   Akers, W.T., Grove, M., Harrison, T.M., and Ryerson, F.J. (1993) The instability of

639   rhabdophane and its unimportance in monazite paragenesis. Chemical Geology, 110 (1-

640   3), 169-176, doi:10.1016/0009-2541(93)90252-E.

641   Burnotte, E., Pirard, E., and Michel, G. (1989) Genesis of Gray Monazites: Evidence from the

642   Paleozoic of Belgium. Economic Geology, 84 (5), 1417-1429.

643   Cabella, R., Lucchetti, G., and Marescotti, P. (2001) Authigenic monazite and xenotime from

644   pelitic metacherts in pumpellyite actinolite-facies conditions, Sestri Voltaggio zone,

645   Central Liguria, Italy. Canadian Mineralogist, 39 (3), 717-727,

646   doi:10.2113/gscanmin.39.3.717.

647   Carlson, W.D. (2002) Scales of disequilibrium and rates of equilibration during

648   metamorphism. American Mineralogist, 87, 185-204.

649   Chisca, S., Borhan, A.I., and Karin, P. (2009) Radioactive waste treatment and disposal:

650   Phosphates for actinides conditioning. Acta Chemica IASI, 17, 73-84.

651   Clavier, N., and Dacheux, N. (2006) Synthesis, characterization, sintering, and leaching of

652   beta-TUPD/monazite radwaste matrices. Inorganic Chemistry, 45 (1), 765-771.

653   Collins-Waite, D. (1987) Diagenesis of the Cambro-Ordovician Beekmantown group: a

654   petrographic and fluid inclusion study. PhD Thesis, Colgate University, Binghamton

655   (NY), 138 pp.

656   Čopjaková, R., Novák, M., and Franců E. (2011) Formation of authigenic monazite-(Ce) to

657   monazite-(Nd) from Upper Carboniferous graywackes of the Drahany Upland: Roles of

658   the chemical composition of host rock and burial temperature. Lithos, 127 (1-2), 373-

659   385, doi:10.1016/j.lithos.2011.08.001.

660   Dahl, P.S., Terry, M.P., Jercinovic, M.J., Williams, M.L., Hamilton, M.A., Foland, K.A.,

661   Clement, S.M., and Friberg, L.V.M. (2005) Electron probe (Ultrachron)

662   microchronometry of metamorphic monazite: Unraveling the timing of polyphase

663   thermotectonism in the easternmost Wyoming Craton (Black Hills, South Dakota).

664   American Mineralogist, 90, 1712-1728.

665   Daniel, C.G., and Pyle, J.M. (2006) Monazite–xenotime thermochronometry and Al_2SiO_5

666   reaction textures in the Picuris Range, northern New Mexico, USA: New evidence for a

667   1450–1400 Ma orogenic event. Journal of Petrology, 47, 97-118.

668   Elliott, W.C., and Aronson, J.L. (1987) Alleghanian episode of K-benitonite illitization in the

669   southern Appalachian Basin. Geology, 15, 735-739, doi:10.1130/0091-

670   7613(1987)15<735:AEOKII>2.0.CO;2.

671   Evans, J.A., Zalasiewicz, J.A., Fletcher, I.R., Rasmussen, B., and Pearce, N.J.G. (2002)

672   Dating diagenetic monazite in mudrocks: constraining the oil window? Journal of the

673   Geological Society, London, 159, 619-622.

674   Evans, J.A., and Zalasiewicz, J. (1996) U-Pb, Pb-Pb and Sm-Nd dating of authigenic

675   monazite: implications for the diagenetic evolution of the Welsh Basin. Earth and

676   Planetary Science Letters, 144, 421-433.

677   Ewing, R.C., and Wang, L. (2002), Phosphates as Nuclear Waste Forms. Reviews in

678   Mineralogy and Geochemistry, v. 48, no. 1, p. 673-699, doi:10.2138/rmg.2002.48.18.

679   Fisher, D.W. (1968) Geology of the Plattsburgh and Rouses Point New York-Vermont

680   quadrangles. New York State Museum Map and Chart Series, 10, 51 pp.

681   Fisher, D.W. (1977) Correlation of the Hadrynian, Cambrian and Ordovician rocks in New

682   York State. New York State Museum, Map and Chart Series No. 25, 75 pp.

683   Foster, G., Gibson, H.D., Parrish, R.R., Horstwood, M., Fraser, J., and Tindle, A. (2002)

684   Textural, chemical and isotopic insights into the nature and behaviour of metamorphic

685   monazite. Chemical Geology, 191, 183-207.

686   Foster, G., Kinny, P., Vance, D., Prince, C., and Harris, N. (2000) The significance of

687   monazite U-Th-Pb age data in metamorphic assemblages; a combined study of monazite

688   and garnet chronometry. Earth and Planetary Science Letters, 181, 327-340.

689   Friedman, G.M. (1987) Vertical movements of the crust: Case histories from the northern

690   Appalachian Basin. Geology, 15(12), 1130-1133, doi:10.1130/0091-

691   7613(1987)15<1130:VMOTCC>2.0.CO;2.

692   Gibson, H.D., Carr, S.D., Brown, R.L., and Hamilton, M.A. (2004) Correlations between

693   chemical and age domains in monazite, and metamorphic reactions involving major

694   pelitic phases: an integration of ID-TIMS and SHRIMP geochronology with Y–Th–U X-

695   ray mapping. Chemical Geology, 211, 237-260.

696   Gimeno Serrano, M. (2000) REE speciation in low-temperature acidic waters and the

697   competitive effects of aluminum. Chemical Geology, 165 (3-4), 167-180,

698   doi:10.1016/S0009-2541(99)00166-7.

699   Goldstein, A., Selleck, B., and Valley, J.W. (2005) Pressure, temperature, and composition

700   history of syntectonic fluids in a low-grade metamorphic terrane. Geology, 33 (5), 421-

701   424, doi:10.1130/G21143.1.

702   Haas, J.R., Shock, E.L., and Sassani, D.C. (1995) Rare earth elements in hydrothermal

703   systems: Estimates of standard partial molal thermodynamic properties of aqueous

704   complexes of the rare earth elements at high pressures and temperatures. Geochimica et

705   Cosmochimica Acta, 59 (21), 4329-4350, doi:10.1016/0016-7037(95)00314-P.

706   Harlov, D.E., Wirth, R., and Hetherington, C.J. (2007) The relative stability of monazite and

707   huttonite at 300-900 °C and 200-1000 MPa: Metasomatism and the propagation of

708   metastable mineral phases. American Mineralogist, 92 (10), 1652–1664.

709   Heizler, M.T., and Harrison, T.M. (1998) The thermal history of the New York basement

710   determined from $^{40}Ar/^{39}Ar$ K-feldspar studies. Journal of Geophysical Research, vol.

711   103, no. B12, 29795–29814.

712   Hermann, J., and Rubatto, D. (2003) Relating zircon and monazite domains to garnet growth

713   zones: age and duration of granulite facies metamorphism in the Val Malenco lower

714   crust. Journal of Metamorphic Geology, 21, 833-852.

715   Hetherington, C.J., Jercinovic, M.J., Williams, M.L., and Mahan, K.H. (2008) Understanding

716   geologic processes with xenotime: Composition, chronology, and a protocol for electron

717   probe microanalysis. Chemical Geology, 254 (3-4), 133-147,

718   doi:10.1016/j.chemgeo.2008.05.020.

719   Hietpas, J., Samson, S., Moecher, D., and Schmitt, A.K. (2010) Recovering tectonic events

720   from the sedimentary record: Detrital monazite plays in high fidelity. Geology, 38 (2),

721   167-170, doi:10.1130/G30265.1.

722   Jacobi, R.D. (2002) Basement faults and seismicity in the Appalachian Basin of New York

723   State. Tectonophysics, 353, 75–113.

724   Janots, E., Engi, M., Berger, A., Allaz, J., Schwarz, J.O., and Spandler, C. (2008) Prograde

725   metamorphic sequence of REE minerals in pelitic rocks of the Central Alps; implications

726   for allanite-monazite-xenotime phase relations from 250 to 610 degrees C. Journal of

727   Metamorphic Geology, 26 (5), 509-526.

728   Jercinovic, M.J., Williams, M.L., Allaz, J., and Donovan, J.J. (2012), Trace analysis in

729   EPMA. IOP Conference Series: Materials Science and Engineering, v. 32, p. 1-22,

730   doi:10.1088/1757-899X/32/1/012012

731   Jercinovic, M.J., Williams, M.L., and Lane, E.D. (2008) In-situ trace element analysis of

732   monazite and other fine-grained accessory minerals by EPMA. Chemical Geology, 254,

733   197-215, doi:10.1016/j.chemgeo.2008.05.016

734   Landing, E., Amati, L., and Franzi, D.A. (2009) Epeirogenic transgression near a triple

735   junction: the oldest (latest early–middle Cambrian) marine onlap of cratonic New York

736   and Quebec. Geological Magazine, 146 (4), 552-566, doi:10.1017/S0016756809006013.

737   Lev, S.M., McLennan, S.M., Meyers, W.J., and Hanson, G.N. (1998) A Petrographic approach

738   for evaluating trace-element mobility in a black shale. Journal of Sedimentary Research,

739   68 (5), 970-980, doi:10.1306/D42688C4-2B26-11D7-8648000102C1865D.

740   Lev, S.M., McLennan, S.M., and Hanson, G.N. (1999) Mineralogic controls on REE mobility

741   during black-shale diagenesis. Journal of Sedimentary Research, 69 (5), 1071-1082,

742   doi:10.1306/D4268B0D-2B26-11D7-8648000102C1865D.

743   Lewis, A.J., Palmer, M.R., Sturchio, N.C., and Kemp, A.J. (1997) The rare earth element

744   geochemistry of acid-sulphate and acid-sulphate-chloride geothermal systems from

745   Yellowstone National Park, Wyoming, USA. Geochimica et Cosmochimica Acta, 61 (4),

746   695-706, doi:10.1016/S0016-7037(96)00384-5.

747   Lim, C., Kidd, W.S.F., and Howe, S.S. (2005) Late shortening and extensional structures and

748   veins in the Western margin of the Taconic Orogen (New York to Vermont). Journal of

749   Geology, 113 (4), 419-438, doi:10.1086/430241.

750   Mahan, K. H., Wernicke, B.P., and Jercinovic, M.J. (2010) Th-U-total Pb geochronology of

751   authigenic monazite in the Adelaide rift complex, South Australia, and implications for

752   the age of the type Sturtian and Marinoan glacial deposits. Earth and Planetary Science

753   Letters, 289 (1-2), 76-86, doi:10.1016/j.epsl.2009.10.031.

754   McDonough, W.F., and Sun, S.s. (1995) The composition of the Earth. Chemical Geology,

755   120, 223-253.

756   McLelland, J.M., Selleck, B.W., and Bickford, M.E. (2010) Review of the Proterozoic

757   evolution of the Grenville Province, its Adirondack outlier, and the Mesoproterozoic

758   inliers of the Appalachians. In R.P. Tollo, M.J. Bartholomew, J.P. Hibbard, and P.M.

759   Karabinos, Eds., From Rodinia to Pangea: The Lithotectonic Record of the Appalachian

760   Region: Geological Society of America Memoir 206, pp. 1-29.

761   McLennan, S.M. (1989) Rare earth elements in sedimentary rocks: influence of provenance

762   and sedimentary processes. In B.R. Lipin and G.A. McKay, Eds., Geochemistry and

763   mineralogy of rare earth elements, 21, pp. 169-200, Reviews in Mineralogy and

764   Geochemistry, Mineralogical Society of America, Washington D.C.

765   Milodowski, A.E., and Zalasiewicz, J.A. (1991) Redistribution of rare earth elements during

766   diagenesis of turbidite/hemipelagite mudrock sequences of Llandovery age from central

767   Wales. Geological Society of London, Special Publications, 57 (1), 101-124,

768   doi:10.1144/GSL.SP.1991.057.01.10.

769   Montario, M.J., and Garver, J.I. (2009) The thermal evolution of the Grenville Terrane

770   revealed through U Pb and fission-track analysis of detrital zircon from Cambro-

771   Ordovician quartz arenites of the Potsdam and Galway formations. Journal of Geology,

772   117(6), 595-614, doi:10.1086/605778.

773   Montel, J.M., Foret, S., Veschambre, M., Nicollet, C., and Provost, A. (1996) Electron

774   microprobe dating of monazite. Chemical Geology, 131, 37-53.

775   Oelkers, E.H., and Montel, J.M. (2008) Phosphates and nuclear waste storage. Elements, 4,

776   113-116, doi:10.2113/gselements.4.2.113.

777   Oelkers, E.H., and Poitrasson, F. (2002) An experimental study of the dissolution

778   stoichiometry and rates of a natural monazite as a function of temperature from 50 to

779   230 °C and pH from 1.5 to 10. Chemical Geology, 191 (1-3), 73-87, doi:10.1016/S0009-

780   2541(02)00149-3.

781   O'Reilly, C., and Parnell, J. (1999) Fluid flow and thermal histories for Cambrian –

782   Ordovician platform deposits, New York: Evidence from fluid inclusion studies.

783   Geological Society of America Bulletin, 111, 1884-1896, doi:10.1130/0016-

784   7606(1999)111<1884.

785   Overstreet, W.C. (1967) The Geological Occurrence of Monazite. U.S. Geological Survey

786   Professional Paper 530, 327 pp.

787   Parrish, R.R. (1990) U-Pb dating of monazite and its application to geological problems.

788   Canadian Journal of Earth Sciences, 27, 1431-1450.

789   Petrík, I., and Konecný, P. (2009) Metasomatic replacement of inherited metamorphic

790   monazite in a biotite-garnet granite from the Nizke Tatry Mountains, Western

791   Carpathians, Slovakia: Chemical dating and evidence for disequilibrium melting.

792   American Mineralogist, 94 (7), 957–974.

793   Poitrasson, F., Chenery, S., and Bland, D.J. (1996) Contrasted monazite hydrothermal

794   alteration mechanisms and their geochemical implications. Earth and Planetary Science

795   Letters, 145, 79-96.

796   Poitrasson, F., Chenery, S., and Shepherd, T.J. (2000) Electron microprobe and LA-ICP-MS

797   study of monazite hydrothermal alteration: Implications for U-Th-Pb geochronology and

798   nuclear ceramics. Geochimica et Cosmochimica Acta, 64 (19), p. 3283-3297.

799   Poitrasson, F., Oelkers, E., Schott, J., and Montel, J.M. (2004) Experimental determination of

800   synthetic $NdPO_4$ monazite end-member solubility in water from 21°C to 300°C:

801   implications for rare earth element mobility in crustal fluids. Geochimica et

802   Cosmochimica Acta, 68 (10), 2207-2221, doi:10.1016/j.gca.2003.12.010.

803   Polyakov, E.V., Volkov, I.V., Surikov, V.T., Perelyaeva, L.A., and Shveikin, G.P. (2010)

804   Dissolution of Monazite in Humic Solutions. Radiochemistry, 52 (4), 429-434,

805   doi:10.1134/S1066362210040181.

806   Putnis, A., and Austrheim, H. (2010) Fluid-induced processes: metasomatism and

807   metamorphism. Geofluids, 254-269, doi:10.1111/j.1468-8123.2010.00285.x.

808   Rasmussen, B., Fletcher, I.R., and McNaughton, N.J. (2001) Dating low-grade metamorphic

809   events by SHRIMP U-Pb analysis of monazite in shales. Geology, 29 (10), 963-966,

810   doi:10.1130/0091-7613(2001)029<0963:DLGMEB>2.0.CO;2.

811   Rasmussen, B., Fletcher, I.R., and Sheppard, S. (2005) Isotopic dating of the migration of a

812   low-grade metamorphic front during orogenesis. Geology, 33 (10), 773-776,

813   doi:10.1130/G21666.1.

814   Rasmussen, B., and Muhling, J.R. (2007) Monazite begets monazite: evidence for dissolution

815   of detrital monazite and reprecipitation of syntectonic monazite during low-grade

816   regional metamorphism. Contributions to Mineralogy and Petrology, 154 (6), 675-689,

817   doi:10.1007/s00410-007-0216-6.

818   Rasmussen, B., and Muhling, J.R. (2009) Reactions destroying detrital monazite in

819   greenschist-facies sandstones from the Witwatersrand basin, South Africa. Chemical

820   Geology, 264 (1-4), 311-327, doi:10.1016/j.chemgeo.2009.03.017.

821   Rast, N. (1984) The Alleghenian orogeny in eastern North America. Geological Society of

822   London, Special Publications, 14 (1), 197-217, doi:10.1144/GSL.SP.1984.014.01.19.

823   Read, D., Andreoli, M.A.G., Knoper, M., Williams, C.T., and Jarvis, N. (2002) The

824   degradation of monazite: Implications for the mobility of rare-earth and actinide

825   elements during low-temperature alteration. European Journal of Mineralogy, 14 (3),

826   487-498, doi:10.1127/0935-1221/2002/0014-0487.

827   Repetski, J.E., Ryder, R.T., Weary, D.J., Harris, A.G., and Trippi, M.H. (2008) Thermal

828   Maturity Patterns (CAI and %Ro) in Upper Ordovician and Devonian Rocks of the

829   Appalachian Basin. A Major Revision of USGS Map I–917– E Using New Subsurface

830   Collections, U.S. Geological Survey Scientific Investigations Map 3006, 26 pp.

831   Reynolds, R.C., and Thomson, C.H. (1993) Illite from the Potsdam Sandstone of New York: a

832   probable noncentrosymmetric mica structure. Clays and Clay Minerals, 41 (1), 66-72,

833   doi:10.1346/CCMN.1993.0410107.

834   Schärer, U. (1984) The effect of initial ^{230}Th disequilibrium on young U-Pb ages: the Makalu

835   case, Himalaya. Earth and Planetary Science Letters, 67 (2), 191-204, doi:10.1016/0012-

836   821X(84)90114-6.

837   Selleck, B.W. (2008) Stratigraphy, sedimentology and diagenesis of the Potsdam formation,

838   Southern Lake Champlain Valley, New York. New York State Geological Association,

839   Fieldtrip Guidebook, 80th Annual Meeting, p. 1-13.

840   Seydoux-Guillaume, A.-M., Montel, J.-M., Bingen, B., Bosse, V., de Parseval, P., Paquette,

841   J.-L., Janots, E., and Wirth, R. (2012). Low-temperature alteration of monazite: Fluid

842   mediated coupled dissolution–precipitation, irradiation damage, and disturbance of the

843   U–Pb and Th–Pb chronometers. Chemical Geology, 330–331, 140–158.

844   Smith, M.P., Henderson, P., and Campbell, L.S. (2000) Fractionation of the REE during

845   hydrothermal processes: Constraints from the Bayan Obo Fe-REE-Nb deposit, Inner

846   Mongolia, China. Geochimica et Cosmochimica Acta, 64 (18), 3141-3160.

847   Staal, C.R. van, Whalen, J.B., Valverde-Vaquero, P., Zagorevski, A., and Rogers, N. (2009)

848   Pre-Carboniferous, episodic accretion-related, orogenesis along the Laurentian margin

849   of the northern Appalachians. Geological Society of London, Special Publications, 327

850   (1), 271-316, doi:10.1144/SP327.13.

851   Steiger, R.H., and Jäger, E. (1977) Subcommission on geochronology: Convention on the use

852   of decay constants in geo- and cosmochronology. Earth and Planetary Science Letters,

853   36 (3), 359-362.

854   Stern, R.A., and Rayner, N.M. (2003) Ages of several xenotime megacrysts by ID-TIMS:

855   potential reference materials for ion microprobe U-Pb geochronology. Geological

856   Survey of Canada, Current Research, 2003-F1, 7 pp.

857   Storm, L.C., and Spear, F.S. (2002) Taconian and Acadian rims on Southern Adirondack

858   monazites: hydrothermal fluids from Appalachian metamorphism. Geological Society of

859   America Conference, annual meeting, Paper No. 25-11.

860   Tomkins, H.S., and Ross, G.M. (2005) Biogenic and metamorphic monazite in a

861   Neoproterozoic turbidite sequence, Windermere Supergroup, southern B.C.. Geochimica

862   et Cosmochimica Acta, 69 (10), Supplement, p. 20.

863   Vidal, O., De Andrade, V., Lewin, E., Munoz, M., Parra, T., and Pascarelli, S. (2006) P-T-

864   deformation-Fe^{3+}/Fe^{2+} mapping at the thin section scale and comparison with XANES

865   mapping: application to a garnet-bearing metapelite from the Sambagawa metamorphic

866   belt (Japan). Journal of Metamorphic Geology, 24 (7), 669-683. doi:10.1111/j.1525-

867   1314.2006.00661.x

868   Walsh, G.J., Aleinikoff, J.N., and Wintsch, R.P. (2007) Origin of the Lyme Dome and

869   implications for the timing of multiple Alleghanian deformation and intrusive events in

870   Southern Connecticut. American Journal of Science, 307, 168-215,

871   doi:10.2475/01.2007.06.

872   Wan, Y., Song, T., Liu, D., Yang, T., and Yin, X. (2007) Mesozoic monazite in

873   Neoproterozoic metasediments   : Evidence for low-grade metamorphism of Sinian

874   sediments during Triassic continental collision, Liaodong Peninsula , NE China.

875   Geochemical Journal, 41, 47-55.

876   Whitney, P.R., and Davin, M.T. (1987) Taconic deformation and metasomatism in Proterozoic

877   rocks of the easternmost Adirondacks. Geology, 15 (6), 500-503, doi:10.1130/0091-

878   7613(1987)15<500:TDAMIP>2.0.CO;2.

879   Wilby, P.R., Page, A.A., Zalasiewicz, J.A., Milodowski, A.E., Williams, M., and Evans, J.A.

880   (2007) Syntectonic monazite in low-grade mudrocks: a potential geochronometer for

881   cleavage formation? Journal of the Geological Society, London, 164, 53-36.

882   Williams, M.L., Jercinovic, M.J., Harlov, D.E., Budzyń, B., and Hetherington, C.J. (2011)

883   Resetting monazite ages during fluid-related alteration. Chemical Geology, 283 (3–4),

884   218–225.

885   Williams, M.L., Jercinovic M.J., and Heatherington C.J. (2007) Microprobe monazite

886   geochronology: understanding geologic processes by integrating composition and

887   chronology. Annual Review of Earth and Planetary Science, 35, 137-175.

888   Williams, M.L., and Jercinovic, M.J. (2002) Microprobe monazite geochronology: putting

889   absolute time into microstructural analysis. Journal of Structural Geology, 24, 1013-

890   1028.

891   Williams, M.L., Jercinovic, M.J., Goncalves, P., and Mahan K. (2006) Format and philosophy

892   for collecting, compiling, and reporting microprobe monazite ages. Chemical Geology,

893   225 (1), 1-15, doi:10.1016/j.chemgeo.2005.07.024

894   Wintsch, R.P., Kunk, M.J., and Aleinikoff, J.N. (2003) P-T-t paths and differential

895   Alleghanian loading and uplift of the Bronson Hill Terrane, South Central New England.

896   American Journal of Science, 303, 410-446.

897   Wong, M.S., Williams, M.L., McLelland, J.M., Jercinovic, M.J., and Kowalkoski, J. (2011)

898   Late Ottawan extension in the eastern Adirondack Highlands: Evidence from structural

899   studies and zircon and monazite geochronology. Geological Society of America Bulletin,

900   124 (5-6), 857-869. doi:10.1130/B30481.1

901   Zagorevski, A., van Staal, C.R., and McNicoll, V.J. (2007) Distinct Taconic, Salinic, and

902   Acadian deformation along the Iapetus suture zone, Newfoundland Appalachians.

903   Canadian Journal of Earth Sciences, 44 (11), 1567-1585, doi:10.1139/E07-037.

904

905

Figure captions

907

Figure 1: Simplified geological map highlighting the Adirondack massif and the Potsdam
Formation. Sample locations are Ellenburg, NY (EC: 44.8693 N / 73.8146 W); Laphams
Mills, NY (LM: 44.5873 N / 73.5001 W); Putnam Center, NY (PC: 43.7546 N / 73.4071 W);
Wright's Ferry Road, NY (WFR: 43.7992 N / 73.3865 W); Erin, NY (core sample from Olin
#1 well; WNR: 42.1734 N / 76.1855 W).

913

Figure 2: (a) Age versus Th-content in monazite rims. (b) Exponential relation between error
on age, and Pb- or Th-content.

916

Figure 3: WDS compositional mapping in monazite from samples (a-c, e) LM-11 grain m1,
(f-i) PC-2A grain m3, (j-l) EC-3 grain m2, (n-q) WNR-1 grain m6, and (r-u) WNR-3 grain
m6. Green dots in (a), (f), (k), (n) and (r) indicate analyzed area and dates in Ma (2σ error).
(d) Cross-polarized microphotograph of monazite grain in LM-11. (m) Plan-polarized
microphotograph of monazite grain in EC-3. The monazite grains in (d) and (m) are
contoured with a red line, and the detrital core with a dashed red line.

923

Figure 4: Ternary diagrams (LREE) – (HREE+Y) – (thorite/huttonite+cheralite) for (a)
monazite detrital core, (b) rim, and (c) xenotime.

926

Figure 5: REE spectra for (a) detrital cores and (b) rims of monazite normalized to "Moacyr"
(Brazilian monazite reference material). Grey area represents the range of variation (a) for

929   rims and (b) for cores. An average composition of 3 to 12 analyses is used for each spectrum.

930   (c,d) Chondrite normalization using the CI chondrite from McDonough and Sun (1995). A

931   strong negative Eu-anomaly is visible in all monazite cores, but is absent or only weakly

932   negative for monazite rims and xenotime.

933

934   **Figure 6:** (a) Summary of age results for detrital monazite cores. Error (2σ) is equal or less

935   than symbol size. (b) Same results using Gaussian probability curve.

936

937   **Figure 7:** WDS element mapping of U Mβ in grains (a) m1 and (b) m4 of sample PC-6

938   showing the relation between monazite overgrowths and K-feldspar (Kfsp). K-rich phase is

939   visible on these element maps because the peak position of K Kα overlaps that of U Mβ.

940   Kfsp inclusions are restricted to the monazite overgrowth, and the monazite rim preferentially

941   overgrows Kfsp. (c) BSE image highlighting the growth of "fibrous" monazite on a detrital

942   zircon in sample EC-1A.

943

944   **Figure 8:** Cumulative probability plots obtained by summing the Gaussian probability

945   curves, and normalizing to the number of samples considered (n). (a) All data (monazite rims

946   and xenotime), (b) monazite rims, and (c) xenotime. In (b) and (c) data have been split

947   according to the sample location relative to the Adirondack Mountains: northeast (LM, EC),

948   east (PC, WFR) and southern area (WNR). D: deposition time (diagenesis); T: Taconic

949   orogeny; S: Salinic orogeny; Ac: Acadian orogeny; nAc: Neoacadian orogeny; Al:

950   Alleghenian orogeny.

951

952 **Figure 9:** Xenotime overgrowth on zircon in sample PC-6. A late crack has appeared between

953 this overgrowth and the zircon, and is now sealed by chlorite, mixed-clay-interlayer (possibly

954 illite/smectite) and quartz. Inset: WDS compositional map of Th Mα.

955

956

957 **Table captions**

958

959 **Table 1:** Typical quantitative analysis (average on 4 to 8 points) for core and rim monazite in

960 sample LM-11 and PC-6, and for one xenotime in sample PC-6.

961

962 **Table 2:** Synthesis of fluid inclusion studies in the Appalachian region during the Taconic,

963 Acadian, Neo-Acadian and Alleghanian orogenies.

964

965

966 **Data repository**

967

968 **Table DR1:** Complete set of averaged analysis for monazite and xenotime. For rims, row

969 "position" refers to the internal (in), middle (mid) or external (out) rim. 3 to 12 analyses

970 points are averaged in each homogeneous domain. Points showing an obvious difference of

971 chemistry were dismissed. Error on age results is given at 2σ. Eu* and Ce* are respectively

972 Eu- and Ce-anomaly, normalized to chondrite CI (see text).
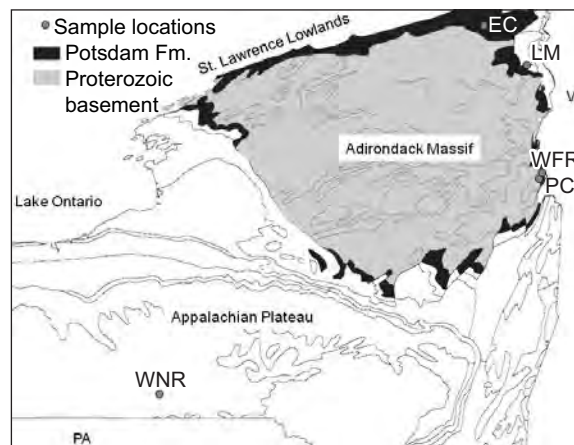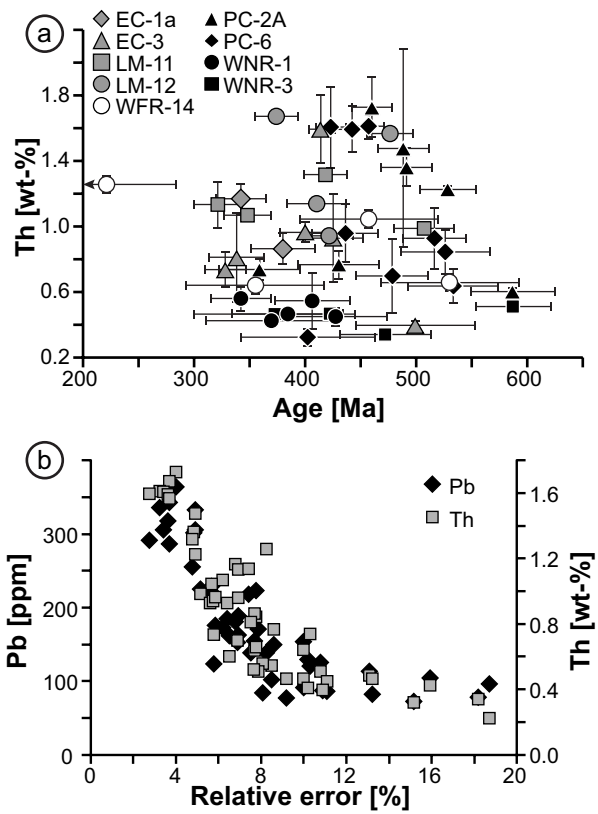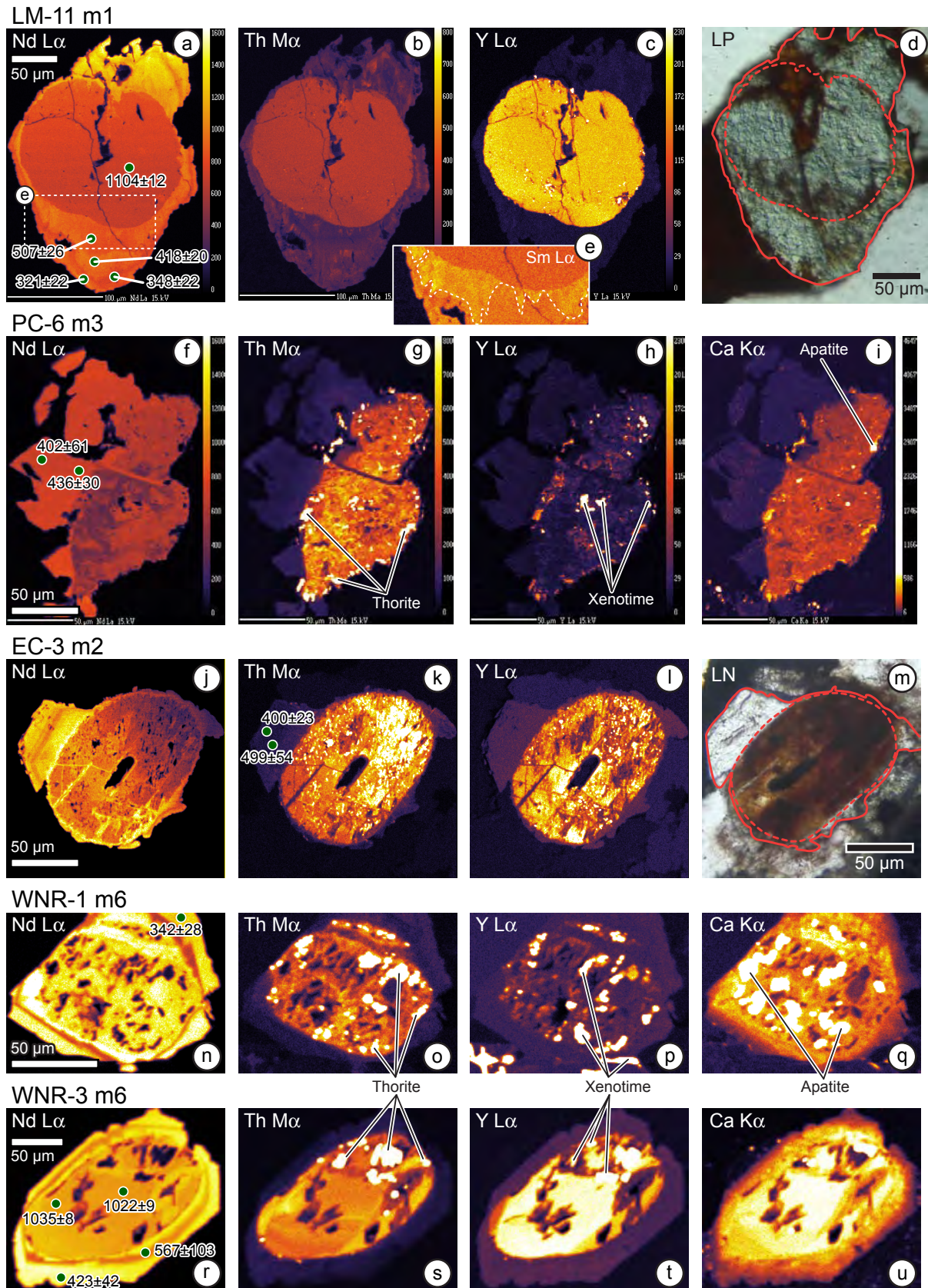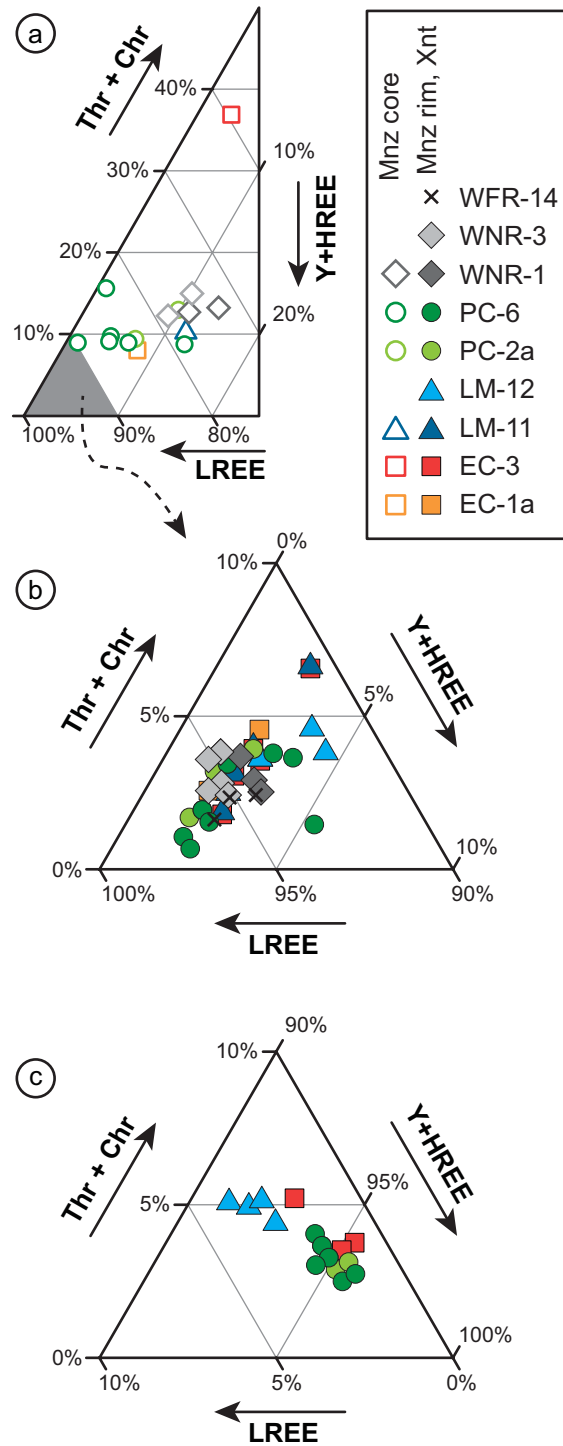
973

974

Figure 1

Figure 2

Figure 3

Figure 4

Figure 5
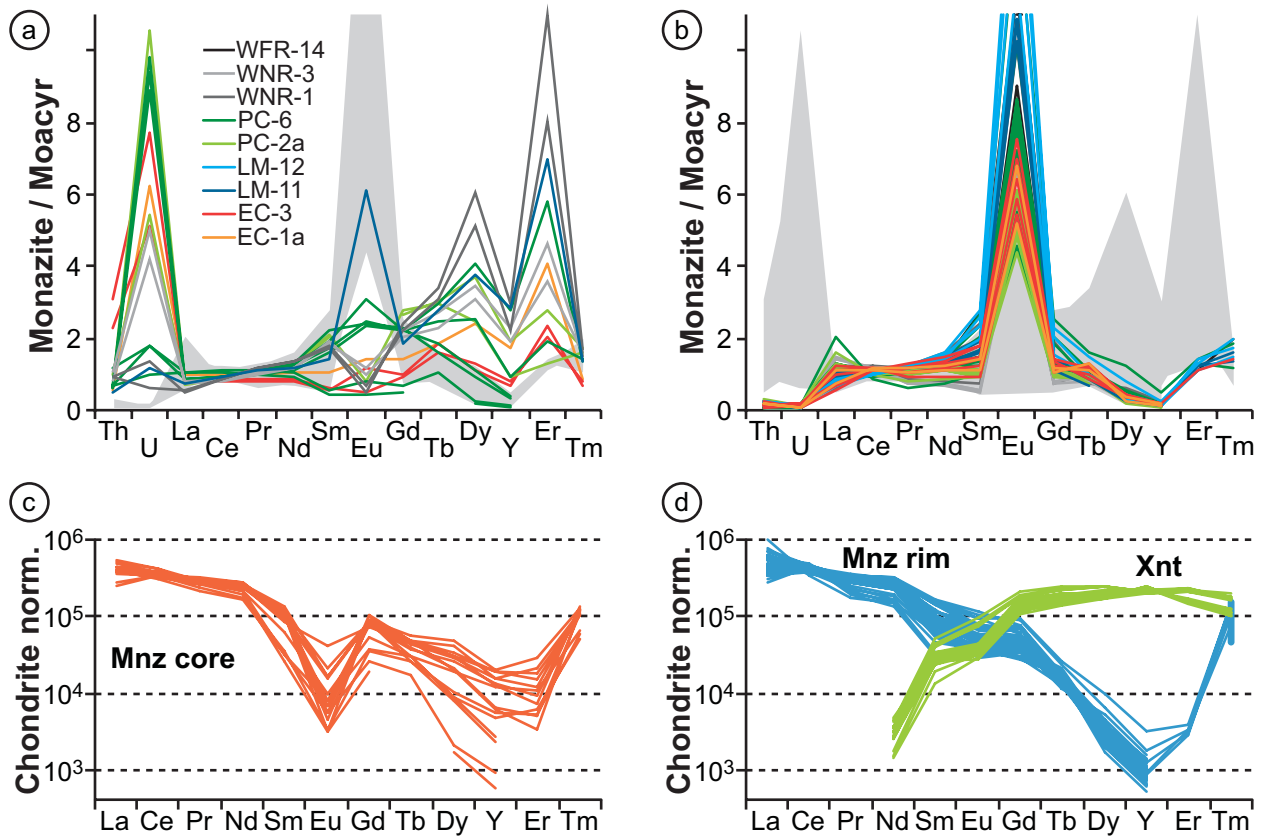
Figure 6
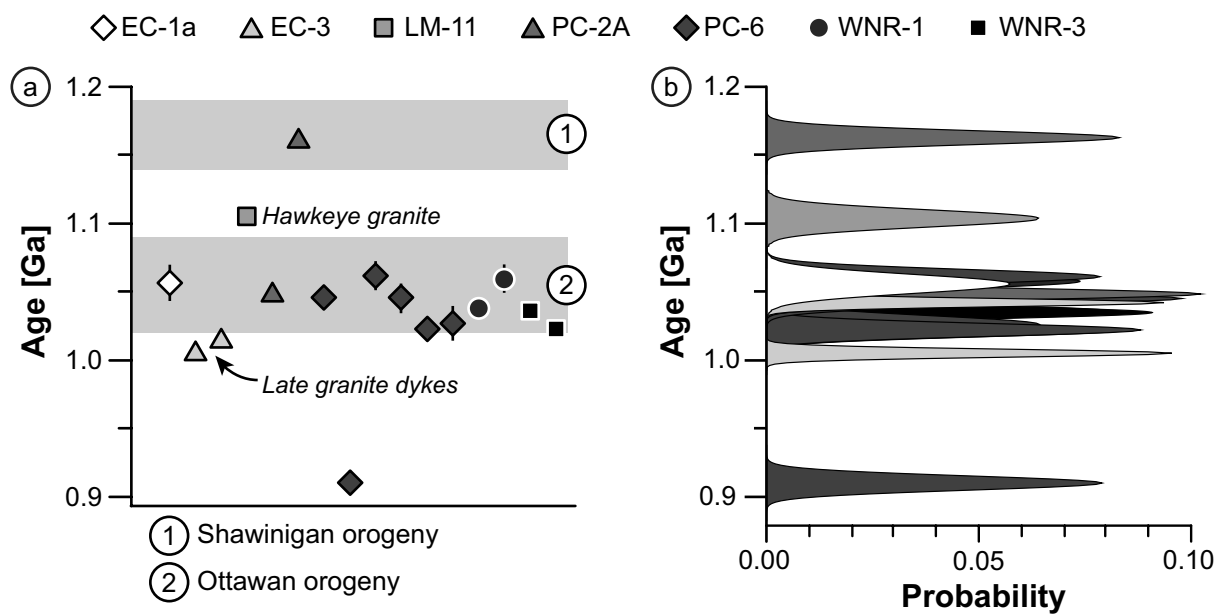
Figure 7
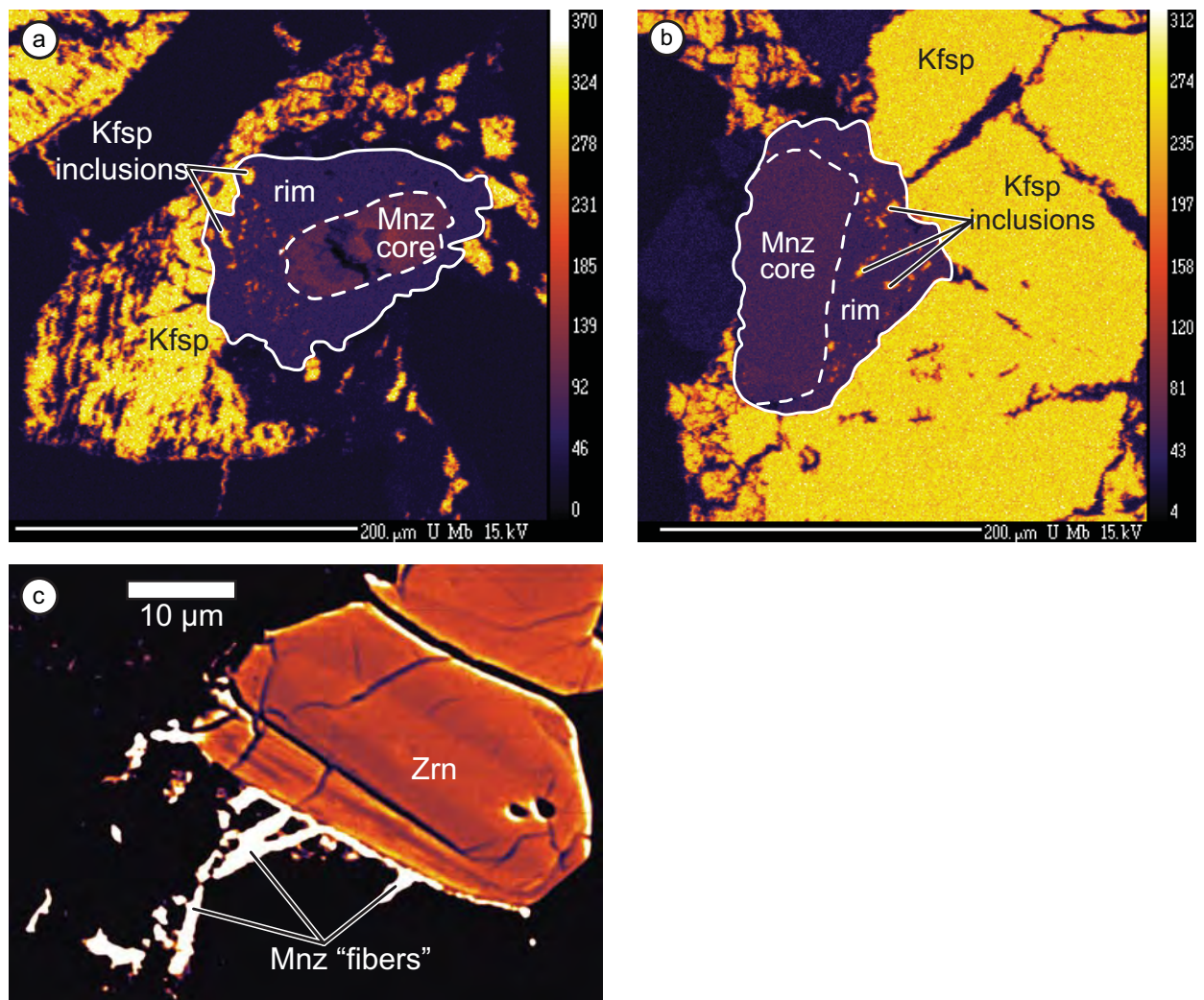
Figure 8
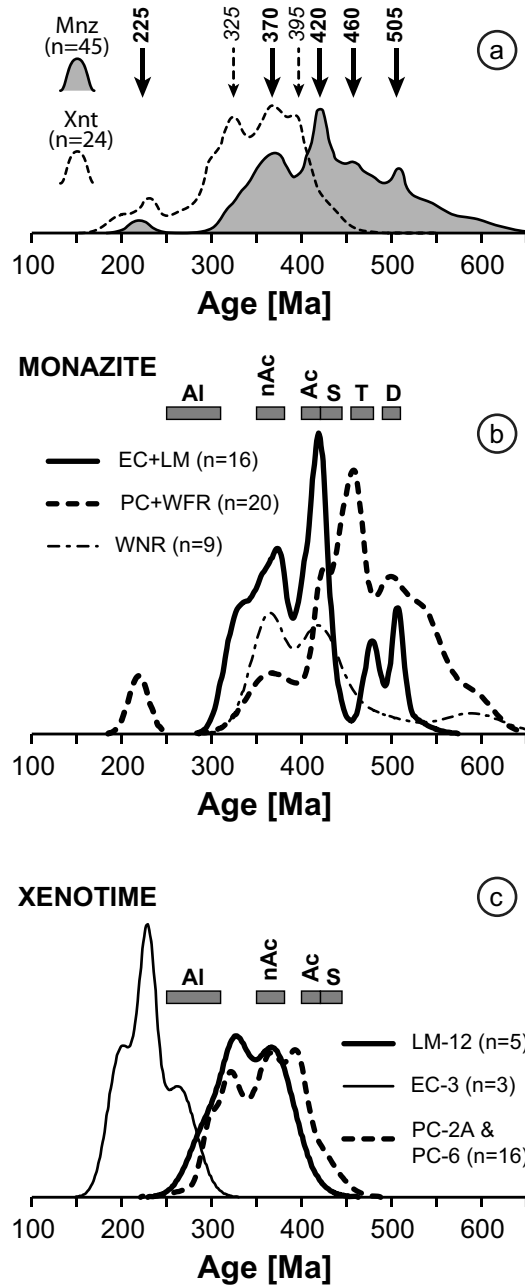
Figure 9
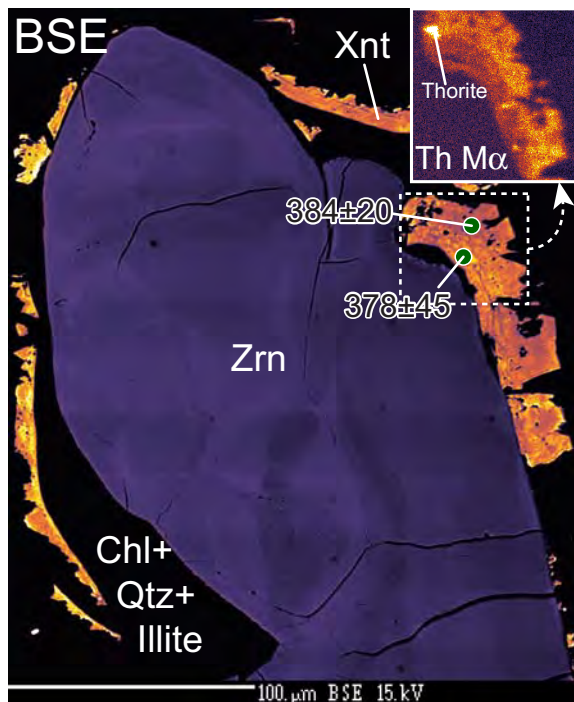
Table 1

Sample	(a) LM-11 (grain m1)					(b) PC-6 (grain m1)		(c) PC-6
Grain	core	rim1	rim2	rim3	rim4	rim1	rim2	x1b rim
Age (Ma)	1104	507	418	321	348	478	442	350
2σ	12	26	20	22	22	33	16	62
P_2O_5	29.15	30.54	30.49	30.30	30.47	29.90	29.27	34.85
Y_2O_3	3.97	0.16	0.17	0.18	0.19	0.15	0.27	48.62
SiO_2	0.91	0.03	0.05	0.15	0.13	0.09	0.30	0.80
CaO	1.12	0.54	0.42	0.14	0.22	0.16	0.20	0.05
La_2O_3	10.72	13.61	11.85	12.03	15.34	18.31	13.71	<0.06
Ce_2O_3	27.94	31.45	31.18	30.98	31.34	30.23	28.81	0.05
Pr_2O_3	3.40	3.61	3.87	3.78	3.51	3.16	3.48	<0.06
Nd_2O_3	13.70	15.21	16.72	16.61	14.42	13.48	16.08	0.15
Sm_2O_3	1.50	1.75	2.05	2.03	1.72	1.54	2.50	0.46
Eu_2O_3	0.27	0.48	0.48	0.52	0.46	0.32	0.45	0.24
Gd_2O_3	1.69	0.97	1.23	1.47	1.23	1.01	1.85	3.35
Tb_2O_3	0.19	0.05	0.06	<0.04	0.08	0.06	0.08	0.66
Dy_2O_3	0.90	<0.04	0.06	0.07	0.09	0.09	0.13	4.90
Ho_2O_3	0.17	<0.10	<0.10	<0.10	<0.10	<0.10	<0.10	0.92
Er_2O_3	0.34	<0.05	0.06	<0.05	0.06	0.06	<0.05	2.88
Tm_2O_3	0.31	0.31	0.36	0.32	0.31	0.27	0.37	0.32
Yb_2O_3	0.13	<0.05	<0.05	<0.05	<0.05	<0.05	<0.05	1.74
ThO_2	3.446	1.119	1.498	1.289	1.214	0.794	1.812	0.711
UO_2	0.098	0.005	0.014	0.003	0.005	0.003	0.003	0.187
PbO	0.180	0.024	0.028	0.018	0.019	0.016	0.034	0.020
K_2O	0.05	0.03	0.05	0.07	<0.03	<0.03	0.06	0.04
SO_2	1.19	0.25	0.06	0.03	0.05	0.02	0.02	0.02
As_2O_3	0.19	<0.15	<0.15	0.19	0.18	<0.15	<0.15	<0.15
SrO	<0.04	0.16	0.14	0.07	0.07	0.08	0.05	<0.04
Total	101.57	100.31	100.86	100.27	101.10	99.74	99.46	100.98

Table 2

Orogeny	Locality	Condition	References
Taconic (480-450 Ma)	Swanton (VT) Samples LM and EC	Low salinity, 5-12% NaCl equivalent, maximum close to carbonate platform	Lim et al. (2005)
	Albany, Whitehall (NY) Samples PC and WFR	170°C (Swanton) to 280°C (Albany, Whitehall)	Lim et al. (2005) Goldstein et al. (2005)
Acadian, Neo-Acadian (420-350 Ma)	Ticonderoga, Whitehall (NY)	Highly saline brines, 16-21% NaCl equivalent 145-225 °C	Collins Waite (1987)
Alleghanian (310-250 Ma)	Southern Appalachian	Highly saline 70-130 °C	Elliott and Aronson (1987)
	Northern Appalachian	Saline fluid Hydrocarbon enrichment	O'Reilly and Parnell (1999)